Unconventional Josephson Effect in Hybrid Superconductor-Topological Insulator Devices

J. R. Williams,[1] A. J. Bestwick,[1] P. Gallagher,[1] Seung Sae Hong,[2] Y. Cui,[3,4] Andrew S. Bleich,[5] J. G. Analytis,[2,4]
I. R. Fisher,[2,4] and D. Goldhaber-Gordon[1]

[1]*Department of Physics, Stanford University, Stanford, California 94305, USA*
[2]*Department of Applied Physics, Stanford University, Stanford, California 94305, USA*
[3]*Department of Material Science, Stanford University, Stanford, California 94305, USA*
[4]*Stanford Institute for Materials and Energy Sciences, SLAC National Accelerator Laboratory, Menlo Park, California 94025, USA*
[5]*Geballe Laboratory for Advanced Materials, Stanford University, Stanford, California 94305, USA*
(Received 18 April 2012; published 30 July 2012)

We report on transport properties of Josephson junctions in hybrid superconducting-topological insulator devices, which show two striking departures from the common Josephson junction behavior: a characteristic energy that scales inversely with the width of the junction, and a low characteristic magnetic field for suppressing supercurrent. To explain these effects, we propose a phenomenological model which expands on the existing theory for topological insulator Josephson junctions.

The Majorana fermion, a charge-neutral particle that is its own antiparticle, was proposed theoretically almost 75 years ago [1]. Electronic excitations in certain condensed matter systems have recently been predicted to act as Majorana fermions [1]. One such system is a three-dimensional topological insulator (TI) where superconducting correlations between particles are introduced, producing a "topological superconductor" [2]. When two superconductors are connected by a TI, the TI "weak link" superconducts due to its proximity to the superconducting leads. This produces a Josephson junction (JJ) but with several important distinctions compared to a conventional JJ, where the weak link is typically an ordinary metal or insulator. Fu and Kane have predicted [2] a one-dimensional (1D) mode of Majorana fermions at the interface between a conventional superconductor and a superconducting topological surface state. Hence, JJs formed with a TI weak link are expected to have two 1D modes at the two superconductor-TI interfaces [arrows in Fig. 1(a)], which fuse to form a 1D wire of Majorana fermions [Fig. 1(a)] running along the width of the device [2]. The energy spectrum of these Majorana fermions is characterized by states within the superconducting gap, which cross at zero energy when the phase difference φ between the two superconducting leads is π.

To probe this exotic state, recent experiments have investigated transport in TI JJs, finding good agreement with conventional JJ behavior [3–7]. Two characteristic properties are typically reported for JJs. The first is the product $I_C R_N$, where I_C is the critical current and R_N is the normal state resistance. $I_C R_N$ should be of order Δ/e (where Δ is the superconducting gap of the leads and e is the charge of the electron) and independent of device geometry [8]. The second characteristic property is the "Fraunhofer-like" magnetic diffraction pattern, i.e., the decaying, oscillatory response of the supercurrent to the magnetic field B,

applied perpendicular to the flow of the supercurrent. The first minimum in I_C should occur at $B = B_C$, when one quantum of flux $\Phi_0 = h/2e$ (where h is Planck's constant) is passed through the area of the device. Recent reports on TI JJs [6,7] match this expectation.

In this Letter we report on transport properties of nanoscale Josephson junctions fabricated using Bi_2Se_3 as the weak link material. The main experimental results of this
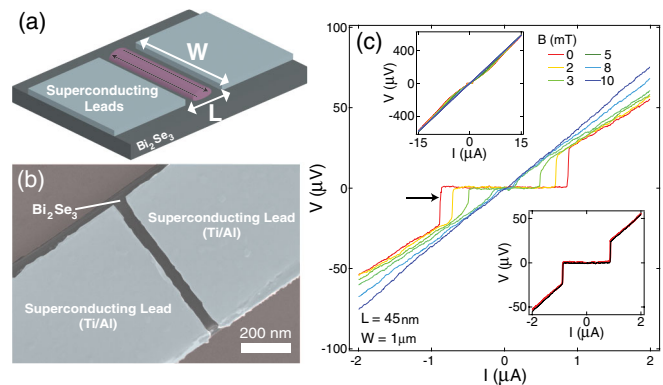

FIG. 1 (color online). (a) Schematic of a topological insulator Josephson junction. Two superconducting leads are patterned on top of Bi_2Se_3 forming a junction with length L and width W. Along the width of the device, resulting in a one-dimensional wire of Majorana fermions (in between superconducting leads). (b) Scanning-electron micrograph of a device similar to the ones measured in this Letter. (c) (main) V vs I for a devices of dimensions $(L, W) = (45$ nm, 1 μm) for $B = 0, 2, 3, 5, 8, 10$ mT and at a temperature of 12 mK. At $B = 0$, I_C is 850 nA, which is reduced upon increasing B. For this device, the product $I_C R_N = 30.6$ μV, much lower than theoretically expected for conventional JJs. (upper-left inset) I-V curves overlap for all values of B at $V \gtrsim 2\Delta/e \sim 300$ μV. (lower-right inset) Sweeps up and down in I show little hysteresis, indicating that the junction is in the overdamped regime.

Letter are two departures from conventional Josephson junction behavior in these devices: a small value of $I_C R_N$ that scales inversely with the width of the junction; and a value of B_C that is ~5 times smaller than that expected from the device area. Neither of these results is predicted or previously seen for conventional JJs nor TI JJs. To explain these experimental observations, we propose a twofold phenomenological extension to the model in Ref. [2], with both extensions arising from confinement along the length of the 1D Majorana wire.

To investigate the properties of JJs with TI weak links, junctions of lengths L between 20 and 80 nm and widths W between 0.5 and 3.2 μm were fabricated via electron-beam lithography and sequential deposition of Ti followed by Al to form electrical leads [9] [Fig. 1(b)]. The dc response for a $(L, W) = (45$ nm, 1 μm) junction at a temperature of 12 mK is shown in Fig. 1(c), where the dc voltage (V) is plotted as a function of the applied dc current (I). At $B = 0$, a typical dc Josephson response is observed (indicated with arrow): for $|I| \leq I_C = 850$ nA, $V = 0$ and a supercurrent flows. Applying B perpendicular to the top surface of the Bi$_2$Se$_3$ reduces I_C until $B = 10$ mT when the superconducting leads are driven normal and the I-V curve becomes linear. For $I > I_C$, there is an excess current due to Cooper pairs leaking into a low-barrier junction [10]; this excess decreases with B. For $V \geq 2\Delta/e \sim 300$ μV, all curves fall on top of each other [upper-left inset of Fig. 1(c)] for all values of B. Absence of hysteresis [lower-right inset of Fig. 1(c)], indicates that the junction is overdamped, consistent with calculations [9]. R_N for this device is 35 Ω and $I_C R_N = 30.6$ μV. Measurements of R_N were carried out above the superconducting transition temperature of the leads in a four-terminal geometry, eliminating the resistance of the cryostat lines, but not the contact resistance between Ti/Al and Bi$_2$Se$_3$, which varies from device to device without apparent correlation to geometry or effect on $I_C R_N$ product. Theory [11] for diffusive or ballistic weak links predicts $I_C R_N$ to be 281 or 427 μV, respectively, an order of magnitude higher than our measurements. As a control experiment, a device fabricated similarly to the TI JJs, except with a 75 nm-thick graphite weak link in place of Bi$_2$Se$_3$, has $I_C R_N = 244$ μV [9], much closer to theoretical predictions. This suggests that something in the sample rather than the measurement setup reduces the values of $I_C R_N$.

Further insight into the nature of transport in TI JJs is found by investigating the width dependence of the characteristic quantity $I_C R_N$. A comparison of two junctions with $R_N = 56.1$ and 51.5 Ω, and $W = 1$ and 0.5 μm (both $L = 50$ nm), is shown in Fig. 2(a), where the 0.5 μm device has roughly twice the critical current. The mismatch of the I-V curves above I_C is due to the excess current mentioned in connection with Fig. 1(c) (inset), which is typically of order I_C [11] and hence larger in the $W = 0.5$ μm device. The two curves approach each other as V approaches $2\Delta/e$ [inset

Fig. 2(a)]. The values of $I_C R_N$ for all 14 devices we measured that superconduct are shown as a function of $1/W$ in Fig. 2(a). The trend is clear: a larger W produces a smaller $I_C R_N$. With benefit of hindsight, results of some previously reported experiments on TI JJs are consistent with $I_C R_N$ being related to $1/W$, and these are plotted alongside our data in shaded gray shapes outlined in black [Fig. 2(b)]. Specifically: in narrow topological insulator nanowires $I_C R_N$ is relatively high (triangle) [4], though still well below predictions; for intermediate values of W similar to ours, $I_C R_N$ is low (square) [3]; in very wide junctions no supercurrent is observed at all (star) [5]. To account for the different superconducting material used for the contacts, the value of $I_C R_N$ was scaled by the ratio of the superconducting gap of aluminum to superconducting gap of the material used in Ref. [5] (indium) and Ref. [4] (tungsten). Naively, $I_C R_N \propto \Delta$; also in the model we will introduce later, $I_C R_N \propto \Delta$ though with a smaller geometry-dependent prefactor.

The last characteristic response of TI JJs considered in this Letter is the magnetic diffraction pattern (MDP); our devices display an atypical relationship between I_C and B. Figure 3(a) shows the differential response $dV/dI(B, I)$ for
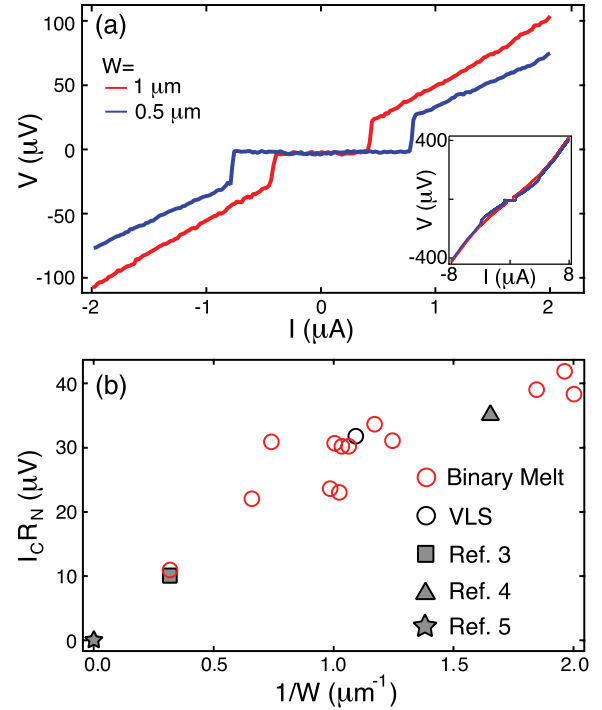

FIG. 2 (color online).   (a) A comparison of two devices with similar R_N (56.1 and 51.5 Ω) and different widths W, 0.5, and 1 μm. The device with $W = 0.5$ μm exhibits a larger I_C, in contrast to conventional JJs, where similar resistances lead to similar values of I_C. (b) $I_C R_N$ vs $1/W$ for all 14 devices (synthesized via two methods: a binary melt and VLS) showing the general trend of $I_C R_N \propto 1/W$. In addition, $I_C R_N$ data points from Refs. [3–5] (symbols) are shown in comparison to the results of this Letter.

a $(L, W) = (55 \text{ nm}, 1.5 \text{ }\mu\text{m})$ device. Two phenomena are of note: B_C is 5 times smaller than expected from the known device area and the shape of $I_C(B)$ deviates from a typical Fraunhofer pattern. The area of the devices is calculated as $W(L + 2\lambda_L)$, where $\lambda_L = 50$ nm is the dirty London penetration depth for aluminum [9]. The extracted $I_C(B)$ is shown in Fig. 3(b) (dashed line with circles) and compared to the simulated Fraunhofer pattern (solid line) for the device area [9]. B_C for this device is 1.70 mT, whereas it should be 9.3 mT, based on the device area measured from a scanning-electron micrograph. We have measured a smaller-than-expected value of B_C in all our devices. The three minima in I_C on each side of $B = 0$ are unequally spaced, occurring at $B = 1.70$, 6.25, and 11.80 mT. Even if the effective area of the junction were larger for unknown reasons, fitting the central peak to a Fraunhofer pattern would produce minima at 1.7, 3.4, and 5.1 mT, different
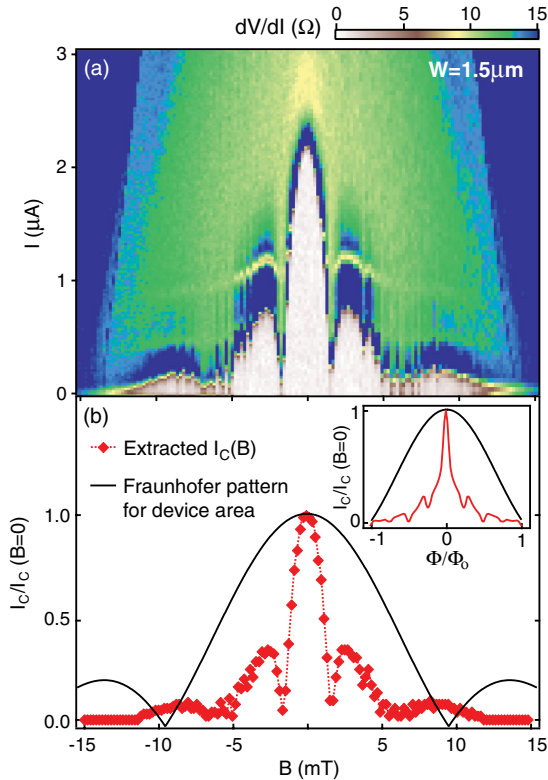
from what is observed. The graphite control device exhibits a more conventional MDP [9], with the first minimum close to the expected field.

We have been unable to explain these experimental observations using known phenomena of conventional JJs, such as Pearl effects, flux focusing, and many others. It is not uncommon to observe reduced values of $I_C R_N$ in conventional JJs because of poor electric contact to the superconductor, thermal fluctuations or activation, or an extra normal channel that does not participate in supercurrent [8]. Nor is it uncommon to have the first minimum of the MDP not at the expected field, because of flux focusing or nonuniform current distribution [12]. Even considering all these effects, and others, as discussed in detail in the Supplemental Material [9], we are not able to account for such large deviations from naive expectations, with consistent behavior over many devices. We therefore instead attempt to account for the effects seen in our Bi_2Se_3 devices in the framework of the model in Ref. [2]. Since the original proposal did not consider our exact geometry or measurement, we propose a twofold phenomenological extension to the model in Ref. [2]: we do not claim to have proven that this phenomenological picture is correct, but since it accounts in an economical way for some of our striking observations we offer it as a spur to further theoretical and experimental work on this system.

First we take into account confinement along the 1D Majorana wire, quantizing its energy levels at multiples of $E_C = h\nu_{\text{ex}}/2l$, with ν_{ex} the velocity of the carriers in the wire and l the length of the wire. In the present devices, the length of the wire is either the width W of the JJ or, if the Majorana modes exist all the way around the TI flake, $2W + 2t$ (where $t \ll W$ is the thickness of the flake), hence $E_C \propto h\nu_{\text{ex}}/2W$. The effect of this quantization on the energy levels is shown in Fig. 4(a). If the $E = 0$ state
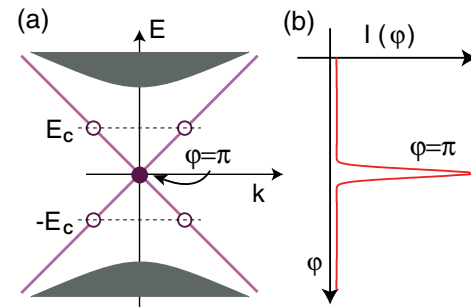

FIG. 3 (color online).   (a) Differential resistance dV/dI as a function of B and I showing an anomalous magnetic diffraction pattern for a $W = 1.5$ μm junction. Two features are of note: a smaller-than-expected value of B_C at 1.70 mT and a nonuniform spacing between minima at values $B = 1.70$, 6.50, 11.80 mT. (b) (main) $I_C(B)$ (dashed line with circles) extracted from dV/dI in (a) is compared to the expected Fraunhofer pattern for the junction (solid line) where a reduction of the scale of the pattern and the nonuniform spacing are evident. (inset) A comparison of the simulated Frauhofer pattern for a sinusoidal and an empirically determined, peaked CPR. The narrowing of the diffraction pattern and the aperiodic minima observed in (a) are captured this CPR.

FIG. 4 (color online).   (a) Energy levels near $\varphi = \pi$ before momentum quantization along W (solid line) and after, where the topological state remains at $E = 0$ (solid circle) and the first quantized energy level at the value E_C (empty circle). (b) Current-phase relation resulting from momentum quantization, producing an anomalous peak at $\varphi = \pi$. The location and shape of the peaks in the current-phase relation depend on the details of energy spectrum of the Andreev bound pairs and in [9] we consider several possible scenarios for this spectrum.

[Fig. 4(a), solid purple dot] is topological in nature; i.e., it is a neutral Majorana mode, such confinement should not affect its existence nor change its energy from zero [13]. The continuum of energy levels at $E \neq 0$, not protected from perturbations, is quantized in multiples of E_C [Fig. 4(a), empty purple dots where only the first non-zero-energy modes are shown for clarity].

The second extension of Ref. [2] is to postulate the supercurrent is dictated by the physics of the junction near the zero-energy ($E = 0$) crossings, whereas when higher-energy modes can be accessed (i.e., when $IR_N \geq E_C/e$) the transfer of carriers from one lead to the other is dissipative. Thus $I_C R_N$ set by the energy scale of confined modes along the width of the junction, rather than by Δ/e: $I_C R_N \propto E_C/e = h\nu_{\mathrm{ex}}/2eW$. There is disagreement in the literature on the relationship between ν_{ex} and ν_F. However, in both available predictions the relationship is of the form $\nu_{\mathrm{ex}} = \nu_F(\Delta/\mu)^n$, where μ is the chemical potential and $n = 2$ in Ref. [2] and $n = 1$ Ref. [14]. As shown in [9], the result of [2] would give energies far too low to account for our observations, so we arrive at the relationship $I_C R_N \propto \Delta$ as in conventional JJs, but with different constants of proportionality, some relating to the geometry of the device.

The confinement would also has an effect on the current-phase relation (CPR), which determines the supercurrent through the device as a function of φ. The supercurrent enabled by the $E = 0$ state occurs at $\varphi = \pi$, producing a sharp peak in the CPR at $\varphi = \pi$ [Fig. 4(b)], in contrast with the established sinusoidal CPR for conventional JJs [8], or a doubled-period sinusoid predicted for TI JJs [15]. The locations and shapes of the peaks in the CPR depend on the details of the energy spectrum of the bound electron-hole pairs, as discussed further in [9].

As described above, the result of confinement is to separate in energy the $E = 0$ 1D modes (neutral Majorana modes) from the $E \neq 0$ (charged) 1D modes. A supercurrent can pass through a charged 1D mode, but the critical current is strongly suppressed by interactions between charges [16,17]. Thus the supercurrent associated with the zero crossing should be larger than that associated with the charged modes at higher energy. In our experiment the lowest-energy charged modes are accessed when the current associated with the zero mode is $\sim 1 \mu$A. We estimate that the charged modes cannot carry this much supercurrent. Hence the charged modes in our devices act as resistors carrying current but not supercurrent. When the charged modes become energetically accessible (i.e., for energies $\geq E_C$) they shunt the junction, with an expected 1D-charged-mode shunt resistance greater than $h/4e^2$ [18]. Renormalization group calculations show that for this value of the shunt resistance supercurrent shuts off, and the JJ behaves as a metal [19]. In this model, any additional supercurrent through the bulk (which might be expected in existing TIs, given the finite bulk conductivity) also ceases when the shunt resistance of the surface become energetically accessible.

Additional peaks in the CPR at certain values of φ, suggested by our phenomenological model as noted above, produce a narrowing in the MDP as observed in Fig. 3. We note that an anomalous, peaked CPR has been theoretically predicted for a different device geometry, also a result of the presence of Majorana fermions [20]. In each case, one sharp feature in the CPR occurs for each zero-energy crossing of states in the gap. For a single peak in the CPR, only a single, $B = 0$ maximum in the MDP is possible for $|\Phi| < \Phi_0$ [9]. The existence of multiple oscillations in $I_C(B)$ for $|\Phi| < \Phi_0$ strongly suggests the presence of multiple peaks in the CPR—possibly a result of coupling to fermionic modes in the device that create additional zero-energy crossings [21]. Through simulation, we are able to show that a smoothly varying CPR cannot capture our results [9] and only a CPR with peaks can create a MDP even coarsely resembling those observed in our devices; i.e., we cannot describe our MDPs using conventional effects like flux focusing or nonuniform supercurrent distribution alone.

When considering the MDP, it is important to note that known topological insulators including Bi_2Se_3 and Bi_2Te_3 have contributions to conductance from both the bulk and the anomalous surface state; both must taken into account when considering supercurrent flow and the CPR of the Josephson junction. A MDP derived from a peaked CPR (from the surface state) added to a conventional, sinusoidal CPR from the bulk with $1/5$ of the amplitude of the surface state [9] is compared to the typical Fraunhofer pattern in the inset of Fig. 3(b). Some, but not all, of the features observed in the experiment are captured by this CPR. Importantly, two features are captured by this peaked CPR: the MDP is narrowed, and nonuniformly distributed minima occur at $\Phi_0/4$, $\Phi_0/2$, and Φ_0 [9], near the aperiodic structure of the minima seen in the experiment. In our materials, a significant effort has been made to reduce the bulk contribution to conductance [22,23]. A systematic investigation of the effect of a bulk supercurrent contribution to the MDP is performed in Ref. [9], where it is found that for roughly equal contributions of the surface and bulk to the CPR, a more conventional MDP results with minor deviations from a Fraunhofer pattern. For example, deviations from a Fraunhofer pattern generated in the simulations of Ref. [9], such as a triangular-shaped central node, can be observed in Ref. [6].

P H Y S I C A L   R E V I E W   L E T T E R S

[1] F. Wilczek, Nature Phys. **5**, 614 (2009).

[2] L. Fu and C. L. Kane, Phys. Rev. Lett. **100**, 096407 (2008).

[3] B. Sacépé, J. B. Oostinga, J. Li, A. Ubaldini, N. J. G. Couto, E. Giannini, and A. F. Morpurgo, Nature Commun. **2**, 575 (2011).

[4] D. Zhang, J. Wang, A. M. DaSilva, J. Sue Lee, H. R. Gutierrez, M. H. W. Chan, J. Jain, and N. Samarth, Phys. Rev. B **84**, 165120 (2011).

[5] J. Wang et al., Phys. Rev. B **85**, 045415 (2012).

[6] F. Qu et al., arXiv:1112.1683.

[7] M. Veldhorst et al., Nature Mater. **11**, 417 (2012).

[8] M. Tinkham, Introduction to Superconductivity (Dover Publications, Mineola, New York 1996).

[9] See Supplemental Material at http://link.aps.org/supplemental/10.1103/PhysRevLett.109.056803 for further details on the device fabrication, superconducting properties of Bi_2Se_3 Josephson Junctions, and simulation of the MDP.

[10] K. Flensberg, J. Bindslev Hansen, and M. Octavio, Phys. Rev. B **38**, 8707 (1988).

[11] K. K. Likharev, Rev. Mod. Phys. **51**, 101 (1979).

[12] A. Barone and G. Paternò, Physics and Applications of the Josephson Effect (Wiley-Interscience Publications, Canada 1982).

[13] A. Kitaev, Phys. Usp. **44**, 131 (2001).

[14] M. Titov, A. Ossipov, and C. W. J. Beenakker, Phys. Rev. B **75**, 045417 (2007).

[15] L. Fu and C. L. Kane, Phys. Rev. B **79**, 161408 (2009).

[16] R. Fazio, F. W. J. Hekking, and A. A. Odintsov, Phys. Rev. Lett. **74**, 1843 (1995).

[17] D. L. Maslov, M. Stone, P. M. Goldbart, and D. Loss, Phys. Rev. B **53**, 1548 (1996).

[18] C. L. Kane and M. P. A. Fisher, Phys. Rev. Lett. **68**, 1220 (1992).

[19] G. Schon and A. D. Zaikin, Phys. Rep. **198**, 237 (1990).

[20] P. A. Ioselevich and M. V. Feigel'man, Phys. Rev. Lett. **106**, 077003 (2011).

[21] K. T. Law and P. A. Lee, Phys. Rev. B **84**, 081304 (2011).

[22] J. G. Analytis, R. D. McDonald, S. C. Riggs, J.-H. Chu, G. S. Boebinger, and I. R. Fisher, Nature Phys. **6**, 960 (2010).

[23] H. Peng, K. Lai, D. Kong, S. Meister, Y. Chen, X.-L. Qi, S.-C. Zhang, Z.-X. Shen and Y. Cui, Nature Mater. **9**, 225 (2010).